JACS
JOURNAL OF THE AMERICAN CHEMICAL SOCIETY
Communication
pubs.acs.org/JACS

Facile Synthesis of Iridium Nanocrystals with Well-Controlled Facets Using Seed-Mediated Growth

Xiaohu Xia,[†] Legna Figueroa-Cosme,[‡] Jing Tao,[§] Hsin-Chieh Peng,[‡] Guangda Niu,[†] Yimei Zhu,[§] and Younan Xia*[,†,‡]

[†]The Wallace H. Coulter Department of Biomedical Engineering, Georgia Institute of Technology and Emory University, Atlanta, Georgia 30332, United States

[‡]School of Chemistry and Biochemistry, Georgia Institute of Technology, Atlanta, Georgia 30332, United States

[§]Condensed Matter Physics & Materials Science Department, Brookhaven National Laboratory, Upton, New York 11973, United States

Supporting Information

ABSTRACT: Iridium nanoparticles have only been reported with roughly spherical shapes and sizes of 1−5 nm, making it impossible to investigate their facet-dependent catalytic properties. Here we report for the first time a simple method based on seed-mediated growth for the facile synthesis of Ir nanocrystals with well-controlled facets. The essence of this approach is to coat an ultrathin conformal shell of Ir on a Pd seed with a well-defined shape at a relatively high temperature to ensure fast surface diffusion. In this way, the facets on the initial Pd seed are faithfully replicated in the resultant Pd@Ir core−shell nanocrystal. With 6 nm Pd cubes and octahedra encased by {100} and {111} facets, respectively, as the seeds, we have successfully generated Pd@Ir cubes and octahedra covered by Ir{100} and Ir{111} facets. The Pd@Ir cubes showed higher H_2 selectivity (31.8% vs 8.9%) toward the decomposition of hydrazine compared with Pd@Ir octahedra with roughly the same size.

Nanocrystals of the Pt-group metals with a face-centered cubic structure (i.e., Pt, Pd, Rh, and Ir) have received particular interest in recent years because of their outstanding performance in a vast variety of industrially important catalytic reactions.[1] It is well-documented that the activity and selectivity of such nanocrystals for a structure-sensitive reaction are highly dependent on the arrangement of atoms and thus the type of crystallographic planes on the surface, which has a strong correlation with the shape.[2] In the oxygen reduction reaction, for example, the catalytic activity of 6 nm Pd cubes enclosed by {100} facets with a square lattice was found to be 1 order of magnitude higher than that of 6 nm Pd octahedra encased by {111} facets with a hexagonal lattice.[3] In another example, the hydrogenation of benzene catalyzed by 13 nm Pt cubes encased by {100} facets generated only cyclohexene, whereas both cyclohexane and cyclohexene were observed for 13 nm Pt cuboctahedra covered by a mixture of {111} and {100} facets.[4]

It is well-known that the Pt-group metals are very expensive because of the ever-increasing demand and their extremely low contents in the Earth's crust (typically at a ppb level).[5] In order to reduce the loading amount of these precious metals and thus achieve sustainable use, we need to maximize the performance of their nanocrystals by carefully controlling the shape. To this end, a variety of different shapes have been reported for Pt, Pd, and Rh nanocrystals over the past few decades.[6] However, to the best of our knowledge, there is no literature report on Ir nanocrystals with well-defined shapes. Most of the reported Ir nanocrystals are irregular particles with sizes of 1−5 nm and roughly spherical shapes.[7] The difficulty in generating Ir nanocrystals with well-controlled facets can be attributed to their small sizes. Because of truncations at the corners and edges, the facets on the side faces are too small to be resolved. The small sizes of Ir nanoparticles can be ascribed to the relatively low energy barrier for homogeneous nucleation compared with that for heterogeneous nucleation during synthesis, as a result of which the newly formed Ir atoms in a synthesis tend to self-nucleate and grow into small particles rather than nucleate on the surface of preformed particles to form larger particles.

Herein we demonstrate that nanocrystals exposing well-defined Ir facets can be synthesized using seed-mediated growth, by which Ir atoms resulting from the reduction of Na_3IrCl_6 by ascorbic acid (AA) and ethylene glycol (EG) were added onto the surface of Pd seeds with well-defined shapes. The key to the success of such a synthesis is to conduct the growth at a high enough temperature (e.g., 200 °C), at which the surface diffusion of the Ir adatoms is greatly accelerated. The fast diffusion of Ir adatoms across the Pd surface ensures a layer-by-layer (LbL) growth mode and thus the formation of a conformal coating of Ir. As long as the Ir shell is smooth at the atomic level, the facets on the resultant Pd@Ir core−shell nanocrystals will replicate those on the initial Pd seeds. Therefore, nanocrystals covered by different Ir facets can be readily obtained simply by using Pd nanocrystals with different shapes as the seeds. Specifically, we have successfully synthesized Pd@Ir cubes and octahedra covered by Ir{100} and Ir{111} facets when Pd cubes and octahedra, respectively, were used as the seeds. The facet-dependent catalytic properties of these Ir-based nanocrystals were investigated by employing them as catalysts for the selective generation of H_2 from the decomposition of hydrazine.

Received: June 6, 2014
Published: July 24, 2014

dx.doi.org/10.1021/ja505716v | J. Am. Chem. Soc. 2014, 136, 10878−10881

We started the synthesis with Pd@Ir core−shell cubes enclosed by Ir{100} facets. In a standard procedure, a solution of Na_3IrCl_6 in EG was slowly introduced (2.0 mL/h using a syringe pump) into a mixture containing poly(vinylpyrrolidone) (PVP) as a stabilizer, AA as the reductant, and Pd cubes with an edge length of 6 nm as the seeds, which had been preheated to 200 °C under magnetic stirring [see the Supporting Information (SI) for details]. The 6 nm Pd cubes encased by six {100} facets were prepared in the presence of Br^- as a capping agent using a previously reported procedure.[8] As shown by the transmission electron microscopy (TEM) images in Figure S1A in the SI, the Pd cubic seeds were uniform in terms of both shape and size. Figure 1A shows a typical TEM image of the Pd@Ir core−shell

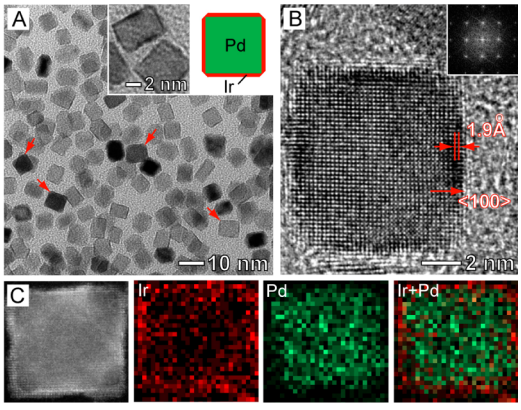

Figure 1. (A) TEM image of Pd@Ir core−shell cubes with slight truncations at the corners. The inset shows a TEM image taken from the same sample at a higher magnification and a 2D schematic model. Red arrows indicate slight truncations at the corner sites. (B) HRTEM image of an individual Pd@Ir cube. The inset is the corresponding FT pattern. (C) HAADF-STEM image of an individual Pd@Ir cube and EDX maps (green = Pd, red = Ir).

cubes prepared using the standard procedure. A thin, conformal Ir shell was formed on the surface of each Pd cubic seed, and the shell can be clearly resolved due to the good contrast between Pd and Ir. It can be seen that the cubic shape of the Pd seeds was fully retained during the deposition of Ir. Our analyses on a large number of particles (>50) indicated that the Pd@Ir cubes had an average edge length of 7.5 nm, which is 1.5 nm greater than that of the initial Pd cubic seeds. Therefore, the thickness of the Ir shell on each Pd{100} facet was 0.75 nm on average. A closer examination indicates that the Pd@Ir cubes had slight truncations at the corners (red arrows in Figure 1A), whose appearance can be attributed to partial desorption of Br^- ions from the side faces of the Pd cubic seeds during the preheating process because of the presence of a reductant.[9] This was validated by the X-ray photoelectron spectroscopy (XPS) data shown in Figure S2. Without the passivation by Br^- ions, the surface free energy of Pd{100} is expected to be higher than that of Pd{111}.[6,9] Therefore, during the growth, Ir atoms tended to preferentially nucleate and grow on the high-energy Pd{100} facets in an attempt to reduce the total free energy of the system, resulting in truncations at the corner sites. This argument was also supported by the result that these slightly truncated Pd@Ir cubes further grew into truncated Pd@Ir cubes with an enlarged truncation area when additional Na_3IrCl_6 was added to the growth solution (Figure S3). We further characterized the structure and composition of the Pd@Ir cubes in Figure 1A by XPS, high-resolution TEM (HRTEM), high-angle annular dark-field scanning TEM (HAADF-STEM), and energy-dispersive X-ray (EDX) mapping. The XPS data (Figure S4) confirm that the shell of the Pd@Ir cubes is composed of Ir(0). The typical HRTEM image of an individual Pd@Ir cube along the [100] zone axis and the corresponding Fourier transform (FT) pattern (Figure 1B) clearly show the Pd@Ir cube to be bounded by Ir{100} facets. The HRTEM image also reveals the continuous lattice fringes from the Pd core to the Ir shell, indicating an epitaxial relationship between the two metals. As the lattice mismatch between Pd and Ir is only 1.3% (3.89 vs 3.84 Å), it was impossible to resolve the elemental compositions from the lattice spacing, and the interfacial strain caused by lattice mismatch can be neglected. We applied EDX analysis to examine the distributions of Pd and Ir in each core−shell cube. The EDX maps (Figure 1C) clearly show a color difference between the core (green = Pd) and the shell (red = Ir), confirming that the shell was dominated by Ir while the core was essentially made of pure Pd.

We believe that fast diffusion of the Ir adatoms during growth was responsible for the formation of a smooth Ir coating and thus the appearance of well-defined Ir facets in the final products. Figure 2A schematically illustrates two possible modes for the

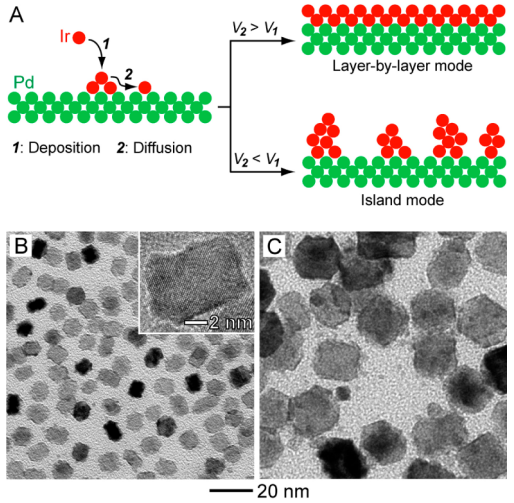

Figure 2. (A) Schematic illustrations of two possible modes of deposition of Ir on Pd cubic seeds. (B, C) TEM images of Pd−Ir bimetallic nanocrystals synthesized using the standard procedure for preparing the Pd@Ir cubes except that (B) the reaction temperature was decreased from 200 to 160 °C and (C) the 6 nm Pd cubic seeds were replaced with the same amount of 18 nm cubic seeds and the volume of Na_3IrCl_6 solution injected was increased from 6 to 20 mL. The inset in (B) is an HRTEM image taken from an individual particle shown in (B).

growth of Ir on Pd cubic seeds. The newly formed Ir atoms are expected to deposit onto the Br^--free Pd(100) surface of a cubic seed because of the relatively high surface energy of Pd{100}. Upon deposition, the Ir adatoms can migrate across the Pd surface by surface diffusion.[10] Only if the rate of surface diffusion is higher than that of atom deposition can the growth proceed by the LbL or Volmer−Weber mode, which gives rise to a smooth, conformal coating of Ir. Otherwise, the growth proceeds by the island or Frank−van der Merwe mode, resulting in the formation of irregular Ir particles on the Pd surface and thus a rough Ir shell. For the present synthesis, Na_3IrCl_6 should be immediately reduced to Ir atoms because of the strong reducing power of AA.[10] Therefore, the concentration of the newly formed Ir atoms in the reaction solution and thereby the deposition rate of Ir is

dx.doi.org/10.1021/ja505716v | J. Am. Chem. Soc. 2014, 136, 10878−10881

mainly determined by the rate of injection of the Na_3IrCl_6 solution, which can be tightly controlled through the use of a syringe pump.[10,11] On the other hand, the rate of surface diffusion can be conveniently varied by adjusting the reaction temperature.[10,11] To validate our assumption, we first decreased the reaction temperature from 200 to 160 °C while keeping the Na_3IrCl_6 injection rate the same as in the standard synthesis (2.0 mL/h). In this case, the rate of surface diffusion decreased, and the Ir adatoms were expected to stay at the deposition sites, facilitating island growth. As expected, Pd−Ir bimetallic nanocrystals with a rough surface were produced as the final products (Figure 2B). A similar morphology was observed when the Na_3IrCl_6 injection rate was increased from 2.0 to 8.0 mL/h while the reaction temperature was maintained at 200 °C (Figure S5). Besides the relatively high rate of surface diffusion, the small size of the Pd cubic seeds (i.e., 6 nm) was also found to contribute to the LbL growth and thus the formation of a smooth, conformal Ir shell. A larger size for the Pd seeds would impose a longer travel distance for the Ir adatoms.[10] As a result, the Ir atoms could not diffuse across the entire Pd surface, leading to island growth and thus the formation of rough Ir shell. For example, Pd−Ir bimetallic nanocrystals with a rough surface were obtained when the 6 nm Pd cubes were replaced by 18 nm Pd cubes as the seeds while all of the other parameters were kept the same as in the standard synthesis except that the volume of Na_3IrCl_6 solution injected was increased from 6 to 20 mL (Figure 2C).

In order to obtain nanocrystals covered by Ir{111} facets, we extended the synthetic strategy from Pd cubes to Pd octahedral seeds encased by eight Pd{111} facets. The procedure for the growth of Ir on Pd octahedral seeds was the same as used for the preparation of Pd@Ir cubes except for the substitution of 6 nm Pd cubes with the same amount of 6 nm Pd octahedra. The uniform 6 nm Pd octahedral seeds (Figure S6) were prepared using citric acid as the capping agent for the Pd{111} facets according to a previously reported method.[3] Figure 3A shows a

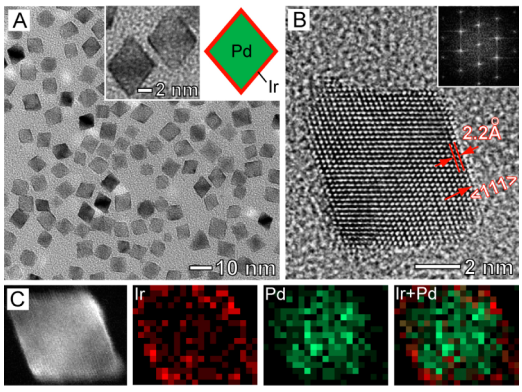

Figure 3. (A) TEM image of Pd@Ir core−shell octahedra. The inset shows a TEM image taken from the same sample at a higher magnification and a 2D schematic model. (B) HRTEM image of an individual Pd@Ir octahedron. The inset is the corresponding FT pattern. (C) HAADF-STEM image of an individual Pd@Ir octahedron together with EDX maps (green = Pd, red = Ir).

TEM image of the as-prepared Pd@Ir core−shell octahedra with an average edge length of 7.8 nm. A thin, smooth Ir shell over the octahedral Pd core can be clearly observed (Figure 3A inset). The typical HRTEM image taken from an individual Pd@Ir octahedron along the [110] zone axis and the corresponding FT pattern (Figure 3B) indicate the exposure of Ir{111} facets on the surface. The core−shell structure was confirmed by the EDX maps (Figure 3C; green = Pd, red = Ir). It is worth pointing out that LbL growth in this case was still maintained even when the reaction temperature was decreased from 200 to 160 °C (Figure S7A), which is different from the case of Pd cubic seeds (Figure 2B). When the reaction temperature was further decreased to 120 °C, the growth was switched to the island mode (Figure S7B). These results indicate that the diffusion rate of Ir adatoms on the Pd(111) surface was higher than on Pd(100) surface at the same temperature. Such a higher diffusion rate can be ascribed to the relatively lower energy barrier for the diffusion of Ir adatoms (E_{diff}) on the Pd(111) surface. In general, a close-packed crystallographic plane such as (111) has a relatively smoother surface and thus a lower E_{diff} than a loose-packed plane with an open structure such as (100) or (110).[12] For example, it was shown that the value of E_{diff} for the diffusion of Rh adatoms is 0.16 eV on the Rh(111) surface and increases to 0.60 and 0.88 eV for Rh(110) and Rh(100), respectively.[12a] Another interesting finding for the growth of Ir on Pd octahedral seeds was that further increasing the volume of Ir precursor solution from 6 to 12 mL (Figure S8) did not result in an increase in the thickness of the Ir shell. Instead, small Ir particles with irregular shapes due to homogeneous nucleation and growth started to appear in the product. This result implies that in the present system the energy barrier for further deposition of Ir atoms on the Ir{111}-covered octahedra is higher than that for the self-nucleation of Ir. We also observed a similar phenomenon, known as self-termination for the growth of the (111) surface, on Pd and Ag octahedra.[13]

Finally, we investigated the facet-dependent catalytic properties of the as-prepared Pd@Ir nanocrystals using selective H_2 generation via the decomposition of hydrous hydrazine as a model catalytic reaction. H_2 generation is at the core of hydrogen fuel cell technology. Hydrous hydrazine, $H_2NNH_2{\cdot}H_2O$, is one of the safest and most efficient hydrogen storage materials, with a hydrogen content as high as 7.9 wt %.[14] It is known that the decomposition of hydrazine has a strong dependence on the type of catalyst used and the reaction conditions.[15] In general, hydrazine can be decomposed in two ways: completely ($H_2NNH_2 \rightarrow N_2 + 2H_2$) and incompletely ($3H_2NNH_2 \rightarrow 4NH_3 + N_2$). Nanoparticles based on Ir were found to be effective in catalyzing the decomposition of hydrazine and the generation of H_2.[16a] Obviously, maximizing the H_2 selectivity for Ir nanocrystals by engineering its surface is expected to be an effective approach to reduce the loading of precious Ir and, at the same time, more efficiently utilize the hydrogen storage material. Nevertheless, it has been extremely difficult to study this subject since essentially none of the reported Ir nanocrystals possess a well-defined shape. The Pd@Ir cubes (Figure 1) and octahedra (Figure 3) covered by Ir{100} and Ir{111} facets, respectively, enabled us to investigate the facet-dependent catalytic properties of Ir nanocrystals toward the decomposition of hydrazine. For comparison, we also prepared Pd@Ir cuboctahedra encased by a mixture of Ir{100} and Ir{111} facets by coating Pd nanospheres with smooth Ir shells (see Figure S9 for details). As shown in Figure 4, all the three types of Pd@Ir core−shell nanocrystals showed catalytic activity toward the decomposition of hydrazine, while essentially no activities were observed for the corresponding Pd seeds. The molar ratios of generated $H_2 + N_2$ to initially added hydrazine were 1.18, 0.73, and 0.57 for the Pd@Ir cubes, cuboctahedra, and octahedra, respectively, corresponding to H_2 selectivities of 31.8%, 14.9%, and 8.9% (see the SI for details). These results indicate that the Ir(100) surface has a much higher H_2 selectivity than the Ir(111) surface toward the decomposition

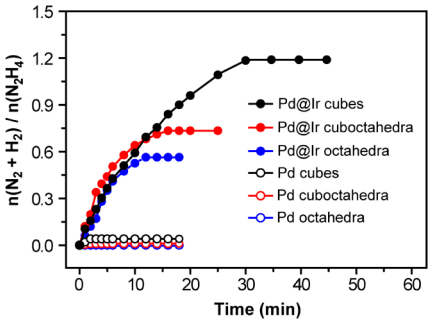

Figure 4. Time course plots for the decomposition of hydrous hydrazine catalyzed by different nanocrystals at room temperature. The *Y* axis is the molar ratio of N_2 + H_2 produced from the reaction to the initially added hydrazine. Each data point represents the average of three independent measurements.

of hydrazine. On the basis of previous reports,[16] the decomposition of hydrazine into N_2 and H_2 on the Ir surface involves a series of steps, including decomposition of adsorbed N_2H_4 into NH_2, splitting of NH_2 into N and H atoms, combination of N and H atoms into N_2 and H_2 molecules, respectively, and finally the desorption of N_2 and H_2 molecules from the Ir surface as gas products. Thus, the observed higher H_2 selectivity for the Ir(100) surface might be attributed to its higher efficiency in facilitating the aforementioned reaction steps compared with the Ir(111) surface. In the future, componential calculations might advance our mechanistic understanding of this catalytic reaction.

In summary, we have demonstrated a facile method based on seed-mediated growth for the synthesis of Ir nanocrystals with well-controlled facets. The essence of this approach is to coat Pd seeds having a well-defined shape with conformal Ir shells to ensure the replication of atomic arrangements on the surface. Both Pd@Ir core−shell cubes and octahedra, enclosed by Ir{100} and Ir{111} facets, respectively, were successfully prepared by using Pd cubes and octahedra as the seeds. The key to the success of this synthesis is to accelerate the rate of surface diffusion for the deposited Ir atoms by increasing the reaction temperature. In comparison with the Ir{111}-covered octahedra, the Ir{100}-covered cubes exhibited a much higher H_2 selectivity toward the decomposition of hydrazine. This work represents the first successful attempt for facet-controlled synthesis of Ir nanocrystals. We believe that the synthetic strategy reported here can also be extended to the synthesis of Ir nanocrystals with other facets by using Pd nanocrystals of different shapes as the seeds.

■ ASSOCIATED CONTENT

Supporting Information

Experimental details, calculation method for H_2 selectivity toward the decomposition of hydrazine, electron microscopy images, and Br 3d XPS spectra. This material is available free of charge via the Internet at http://pubs.acs.org.

■ AUTHOR INFORMATION

Corresponding Author

younan.xia@bme.gatech.edu

Notes

The authors declare no competing financial interest.

■ ACKNOWLEDGMENTS

This work was supported in part by the NSF (DMR-1215034) and startup funds from the Georgia Institute of Technology. Part of the electron microscopy work at BNL was supported by the U.S. Department of Energy, Office of Basic Energy Sciences, Materials Sciences and Engineering Division, under Contract DE-AC02-98CH1088.

■ REFERENCES

(1) (a) Ertl, G. *Handbook of Heterogeneous Catalysis*; Wiley-VCH: Weinheim, Germany, 2008. (b) Zhang, H.; Jin, M.; Xiong, Y.; Lim, B.; Xia, Y. *Acc. Chem. Res.* **2013**, *46*, 1783. (c) Tian, N.; Zhou, Z.; Sun, S.; Ding, Y.; Wang, Z. *Science* **2007**, *316*, 732. (d) Lim, B.; Jiang, M.; Camargo, P. H. C.; Cho, E. C.; Tao, J.; Lu, X.; Zhu, Y.; Xia, Y. *Science* **2009**, *324*, 1302. (e) Nishihata, Y.; Mizuki, J.; Akao, T.; Tanaka, H.; Uenishi, M.; Kimura, M.; Okamoto, T.; Hamada, N. *Nature* **2002**, *418*, 164. (f) Kim, S.-W.; Kim, M.; Lee, W. Y.; Hyeon, T. *J. Am. Chem. Soc.* **2002**, *124*, 7642. (g) Grass, M. E.; Zhang, Y. W.; Butcher, D. R.; Park, J. Y.; Li, Y. M.; Bluhm, H.; Bratlie, K. M.; Zhang, T. F.; Somorjai, G. A. *Angew. Chem., Int. Ed.* **2008**, *47*, 8893. (h) Vidal-Iglesias, F. J.; Solla-Gullón, J.; Montiel, V.; Feliu, J. M.; Aldaz, A. *J. Power Sources* **2007**, *171*, 448.

(2) (a) Narayanan, R.; El-Sayed, M. A. *Nano Lett.* **2004**, *4*, 1343. (b) Langille, M. R.; Personick, M. L.; Zhang, J.; Mirkin, C. A. *J. Am. Chem. Soc.* **2012**, *134*, 14542. (c) Guo, S.; Zhang, S.; Sun, S. *Angew. Chem., Int. Ed.* **2013**, *52*, 8526. (d) Xie, S.; Choi, S.-I.; Xia, X.; Xia, Y. *Curr. Opin. Chem. Eng.* **2013**, *2*, 142.

(3) Shao, M.; Yu, T.; Odell, J. H.; Jin, M.; Xia, Y. *Chem. Commun.* **2011**, *47*, 6566.

(4) Bratlie, K. M.; Kilewer, C. J.; Somorjai, G. A. *J. Phys. Chem. B* **2006**, *110*, 17925.

(5) Jin, R. *Nanotechnol. Rev.* **2012**, *1*, 31.

(6) (a) Xia, Y.; Xiong, Y.; Lim, B.; Skrabalak, S. E. *Angew. Chem., Int. Ed.* **2009**, *48*, 60. (b) Ahmadi, T. S.; Wang, Z. L.; Green, T. C.; Henglein, A.; El-Sayed, M. A. *Science* **1996**, *272*, 1924. (c) Chen, M.; Wu, B.; Yang, J.; Zheng, N. *Adv. Mater.* **2012**, *24*, 862. (d) Sneed, B. T.; Kuo, C. H.; Brodsky, C. N.; Tsung, C.-K. *J. Am. Chem. Soc.* **2012**, *134*, 18417.

(7) (a) Stowell, C. A.; Korgel, B. A. *Nano Lett.* **2005**, *5*, 1203. (b) Fonseca, G. S.; Umpierre, A. P.; Fichtner, P. F. P.; Teixeira, S. R.; Dupont, J. *Chem.—Eur. J.* **2003**, *9*, 3263. (c) Zhang, Y.; Zhang, H.; Zhang, Y.; Ma, Y.; Zhong, H.; Ma, H. *Chem. Commun.* **2009**, 6589. (d) Rueping, M.; Koenigs, R. M.; Borrmann, R.; Zoller, J.; Weirich, T. E.; Mayer, J. *Chem. Mater.* **2011**, *23*, 2008.

(8) Jin, M.; Liu, H.; Zhang, H.; Xie, Z.; Liu, J.; Xia, Y. *Nano Res.* **2011**, *4*, 83.

(9) Peng, H.-C.; Xie, S.; Park, J.; Xia, X.; Xia, Y. *J. Am. Chem. Soc.* **2013**, *135*, 3780.

(10) Xia, X.; Xie, S.; Liu, M.; Peng, H.-C.; Lu, N.; Wang, J.; Kim, M. J.; Xia, Y. *Proc. Natl. Acad. Sci. U.S.A.* **2013**, *110*, 6669.

(11) (a) Xie, S.; Peng, H.-C.; Lu, N.; Wang, J.; Kim, M.; Xie, Z.; Xia, Y. *J. Am. Chem. Soc.* **2013**, *135*, 16658. (b) Xie, S.; Choi, S.-I.; Lu, N.; Roling, L. T.; Herron, J. A.; Zhang, L.; Park, J.; Wang, J.; Kim, M. J.; Xie, Z.; Mavrikakis, M.; Xia, Y. *Nano Lett.* **2014**, *14*, 3570.

(12) (a) Oura, K.; Lifshits, V. G.; Saranin, A.; Zotov, A. V.; Katayama, M. *Surface Science: An Introduction*; Springer: Berlin, 2003; p 333. (b) *Metal-Surface Reaction Energetics: Theory and Applications to Heterogeneous Catalysis, Chemisorption, and Surface Diffusion*; Shustorovich, E., Ed.; Wiley-VCH: Weinheim, Germany, 1991; p 114.

(13) (a) Jin, M.; Zhang, H.; Xie, Z.; Xia, Y. *Energy Environ. Sci.* **2012**, *5*, 6352. (b) Wang, Y.; Wan, D.; Xie, S.; Xia, X.; Huang, C. Z.; Xia, Y. *ACS Nano* **2013**, *7*, 4586.

(14) Schmidt, E. W. *Hydrazine and its Derivatives: Preparation, Properties, Applications*, 2nd ed.; Wiley: New York, 1984.

(15) (a) Singh, S. K.; Zhang, X.-B.; Xu, Q. *J. Am. Chem. Soc.* **2009**, *131*, 9894. (b) Singh, S. K.; Xu, Q. *J. Am. Chem. Soc.* **2009**, *131*, 18032.

(16) (a) Contour, J. P.; Pannetier, G. *J. Catal.* **1972**, *24*, 434. (b) Liu, M.; Zheng, Y.; Xie, S.; Li, N.; Lu, N.; Wang, J.; Kim, M. J.; Guo, L.; Xia, Y. *Phys. Chem. Chem. Phys.* **2013**, *15*, 11822.